

Department of the Geophysical Sciences
The University of Chicago

N64-25573

CODE-1

CAT. 12

NASA CR-56835

Beant

EVALUATION OF LIMB DARKENING FROM TIROS III RADIATION DATA

by

S.H.H. Larsen , T. Fujita, and W.L. Fletcher

XEROX \$
MICROFILM \$

OTS PRICE

2.60 ph



August

1963

DDC

UNCLASSIFIED

501-13657

\$2.60

RESEARCH PAPER #18
MESOMETEOROLOGY PROJECT
Department of the Geophysical Sciences
University of Chicago

EVALUATION OF LIMB DARKENING FROM
TIROS III RADIATION DATA

by

S.H.H. Larsen *, T. Fujita, and W.L. Fletcher

This research was supported by the National Aeronautic and Space Administration under grant NASA Nsg 333, and partially by the Meteorological Satellite Laboratory, United States Weather Bureau, under grant Cwb WBG -6.

* On leave from Oslo University, Institute of Physics.

ABSTRACT

25573

Detailed analyses of radiation data over the Sahara desert, using analog traces (brush records) of the medium resolution, five-channel radiometer on TIROS III, were made in an attempt to evaluate the limb darkening (variation in intensity of outgoing radiation with the direction of propagation). In the technique employed, we made use of the fact that some areas on the earth are scanned twice by the radiometer beam within a few minutes interval as the satellite spins and progresses along its path. Pairs of measurements, where the satellite's radiometer views the same point at a large and a small zenith angle, were combined, and from such measurements a substantial limb darkening was found. Serious influences on the radiation data may occur as a consequence of the scan geometry; these have been carefully examined and taken into account in the interpretation of the data.

A. J. H. H.

I. INTRODUCTION

The meteorological satellite TIROS III carries a five-channel radiometer of about five degree half-power aperture which scans the earth as the satellite rotates. In fig. 1 a schematic view of the TIROS satellite is given which shows the principle of the scanning radiometer. Channels 2 and 4 were designed to measure the intensity of the outgoing terrestrial radiation in the spectral regions at 8 to 12 and 7 to 30 microns respectively. In fig. 2 the spectral response curves of the channels 2, 3 and 4 are drawn on an absorption diagram of the atmosphere in the infrared, presented by Elsasser (1942).

From radiation data obtained by the satellite's measurements in channels 2 and 4, surface temperatures and values of total infrared flux can be deduced. However, radiation registered by channel 2 does not come entirely from the ground or from cloud tops when they are present. According to Hanel and Wark (1961), about 25 percent originates in the lower part of the atmosphere; this must be taken into account in an interpretation of data. Upward radiation is a function of the optical path and the temperature distribution in the atmosphere, and the intensity of the outgoing radiation which is measured by the satellite, depends on the nadir angle of view. When temperature in the atmosphere decreases with height a decrease in the measured intensity of the outgoing radiation occurs as the zenith angle of the line of sight increases. This observed phenomenon is referred to as limb darkening and is a quantitative measure of the anisotropy of the outgoing radiation.

By using model atmospheres the normal range to be expected in limb darkening for channels 2 and 4 has been calculated by Wark, Yamamoto and Lienesch (1962). To substantiate their results it has been necessary to measure the amount of limb darkening by using satellite radiation data. Wark (1963) has made a statistical analysis of satellite radiation data to establish the limb darkening effect which is experienced by the satellite. He first selected

the data in groups according to temperature intervals; next he made a selection according to the nadir angle of view. By this combination of the data he was able to compute a set of limb darkening curves, with each curve representing the specific temperature of the radiating source. A different approach has been taken by us in a thorough examination of the analysed radiation data from one isolated case based on a pass over the Sahara Desert in which the precise rectification technique developed by Fujita (1963a, 1963b and 1963c) has been applied.

II. SATELLITE RADIOMETER MEASUREMENTS

Before we describe the technique involved in our computation of limb darkening some general remarks should be made about the radiometer measurements. The radiation sensed by the five-channel radiometer comes from a relatively small area on the earth, the scope of which is determined by the instrument's aperture. The size and orientation of this area, which is called a scan spot, will continuously vary as the satellite spins and progresses along its path. However, the direction of propagation is nearly constant, relative to the local vertical, during a registration; and dimensionally specific intensity is implicit in any measurement. From calibration measurements the radiometer's response can be converted into a value which represents a filtered flux, \bar{W} , called effective radiant emittance (see NASA radiation manual, 1962). Effective radiant emittance of a target for a sensor is defined as that portion of blackbody radiant emittance which would be detected by a sensor with a spectral response ϕ_ν . The effective radiant emittance may be written:

$$\bar{W} = \int_0^\infty W_\nu(T) \phi_\nu d\nu.$$

Considering isotropic radiation, the specific intensity, I , of the filtered radiation from the target may be written as

$$I = \bar{W}/\pi,$$

and will be given in watts per square meter.

The measured intensity for outgoing terrestrial radiation which originates within the field of view of the radiometer, is a weighted mean over the scan spot. This is a consequence of the variation in sensitivity within the radiometer's aperture. However, \bar{W}/π expresses a measured intensity in one particular direction. In our work with limb darkening we are concerned with an intensity ratio I/I_0 , or the intensity of the outgoing radiation in an oblique direction to the intensity of the outgoing radiation in the vertical. Here the $1/\pi$ factor cancels out; so we present the synoptic maps, used in our computations, according to the measured values of \bar{W} .

III. TECHNIQUE FOR MEASURING LIMB DARKENING

The inclination of the five-channel radiometer's aperture axes are designed to be 45 degrees. When the satellite spins and progresses along its path, its spin axis always points in the same direction in space; as a result, some areas on the earth are scanned twice. The areas are covered by initial and complemental scans of the radiometer beam. A point within such an area will usually be scanned by the radiometer beam at two different zenith angles; this is illustrated in fig. 3. In a pair of measurements like these, we have to consider two different path lengths in the atmosphere where the influence on the upward radiation will be different, so that a measured difference in the outgoing radiation actually expresses the influence of limb darkening. Limb darkening may be defined as the ratio I/I_0 , the ratio of the intensity of outgoing radiation in a direction of zenith angle ζ to the intensity in a direction of zenith angle zero, and is given as a function of ζ . However, from a particular pass just one pair of measurements would provide radiation data to compute the ratio I/I_0 . Therefore it is necessary to introduce an approximate method where we assume no limb darkening exists for outgoing radiation of zenith angles less than 30 degrees.

Thus we may write:

$$I(\zeta)/I(\zeta < 30) = \frac{I(\zeta)}{I(\zeta=0)} \bigg/ \frac{I(\zeta < 30)}{I(\zeta=0)} \approx I(\zeta)/I(\zeta=0) \quad \text{or} \quad I/I_0.$$

On this assumption the ratio $I(\zeta)/I(\zeta < 30)$ will, for different values of ζ , represent limb darkening as a function of the zenith angle ζ , the larger angle in our zenith angle pair.

The measured outgoing radiation, however, is affected by the variations in size and orientation of the scan spots. Such influences are a consequence of the fact that the radiometer always integrates over the area which is viewed. Our data are obtained from pairs of measurements where the radiometer beam, from two different positions of the satellite, is oriented towards the same point on the earth. However, the areas viewed by the radiometer may not be identical. The radiometer beam of the large zenith angle may encompass an area including both hot and cold spots, while the beam of the small zenith angle may strike an area covering only the hot spot; thus two different intensities would be registered by the radiometer even without an intermediate atmosphere. One should realize that the variation in scan spot size is considerable; it may vary from a circle of about sixty miles in diameter to an elliptically shaped area of several hundred miles in major axis. The dimensions of scan spots as a function of the satellite height and zenith angle (as seen from the scan spot) are shown on a scan spot chart by Fujita (1963b).

To minimize this integration defect in our computation, an actual measured value at a small zenith angle is replaced by the weighted mean value from the areas of the corresponding large scan spot. The weighting factor is a sensitivity function of the radiometer. (See Appendic). Also the influence of space contamination should be noted. This contamination starts at a zenith angle of about 80 degrees. Actually, the instrument's field of view is completely filled when the nadir angle of view is less than

$$90^\circ - \delta_H - A/2,$$

where δ_A and A denotes the satellite's dip angle and the radiometer's aperture, respectively.

The actual procedure in the limb darkening computations has been to make two separate analyses over the same geographical area: one based on data obtained when the area is viewed by the satellite at small zenith angles, and the other based on data obtained when the area is viewed at larger zenith angles. Using Fujita's (1963c) terminology, analyses are made from data plotted on initial scan lines and complementary scan lines, respectively. In fig. 4 and 5 the two analyses are shown and the isolines for the zenith angles of satellite are drawn on the maps. Scan spots containing sensitivity contours are constructed, the large scan spots (complementary scan spots) are placed on the synoptic pattern derived from the initial scans, and the weighted mean values are computed. Actual field values are replaced by the computed means, and the same type of "distortion" as that created by the scan geometry in the complementary scan analysis is introduced in the initial scan analysis. After correcting for space contamination, the two analyses are then compared.

The weighted mean radiation values from initial scans provides values at zenith angles less than 30 degrees, just as the radiation pattern from complementary scans, with correction applied for space contamination, provides measured values at the larger zenith angles. We restrict, however, our limb darkening computation within the region of initial scans of zenith angles up to 30 degrees where the zenith angles of complementary scans range from 50 to 90 degrees. Remembering the assumption of no limb darkening as zenith angles up to 30 degrees, we now compute the ratio I/I_0 at ζ equal to 60, 70, 80 and 90 degrees, and these computed values represent our observed limb darkening for this particular case.

IV. RESULTS

The computed values of the ratio of intensity of outgoing radiation at a zenith angle ζ to the intensity of the radiation in the vertical, I/I_0 , or \bar{W}/\bar{W}_0 , in channel 2, at zenith angles of 60, 70, 80 and 90 degrees are plotted against ζ . The smoothed curve through the points gives the observed

range of limb darkening as experienced by the instrument for this particular case. Our values of \bar{W}/\bar{W}_0 are given in table I, and the curve is shown in fig. 6. The observed limb darkening is substantial and exceeds the theoretical values at an increasing rate as the zenith angle increases.

TABLE I. Observed limb darkening channel II, TIROS III over Sahara.

ζ in deg.	\bar{W}/\bar{W}_0	Stand. dev.
60	.93	$\pm .02$
70	.78	$\pm .04$
80	.29	$\pm .04$
90	.19	$\pm .02$

By our method one is able to measure each spot on the earth twice within a few minutes of satellite flight; the results obtained are derived by combining readings from several pair of instruments. Variations in the nature and the temperature of the atmosphere in horizontal planes will affect the measurements and introduce complications, and a calculated standard deviation may include the influence of a nonstratified atmosphere.

For the window region, Beer's law is a good approximation for the atmosphere. If we assume a hot earth surface and a cold atmosphere, we may write:

$$\bar{W}_0/\bar{W} = I_0/I = I_0 e^{-k}/I_0 e^{-k \sec \zeta} ,$$

where I_0 denotes intensity of the upward radiation in the vertical emerging at the top of the atmosphere and I_0 is the intensity of the isotropic radiation emerging at the earth surface. k is the optical thickness of the whole atmosphere for vertical incidence, and we may indicate the transmissivity τ as:

$$\tau = e^{-k} .$$

We have further

$$\text{Log } I_0/I = k(\sec \zeta - 1) ,$$

where the log of the intensity ratio I_0/I is a linear function of $(\sec \zeta - 1)$ under conditions stated above. In a diagram, given in fig. 7, values of the log

intensity ratio, $\log I_0/I$, which are based on our observed values of the intensities of outgoing radiation, I , are plotted against $(\sec \zeta - 1)$; and the values of $\log I_0/I$, based on the calculation of I in model atmospheres by Wark, Yamamoto, and Lienesch (1962), have been plotted in the same diagram.

Up to about 70 degrees zenith angle the values of $\log I_0/I$ based on the I - values of Wark and collaborators are in reasonable agreement with those based on our observed values of I . Above 70 degrees the observed log intensity curve starts to rise, and it deviates from the theoretical values at an increasing rate with increasing ζ . One should remember, however, that the log diagram itself exaggerates, to a certain extent, the deviation between the observed and the theoretical values. It should be pointed out that the atmospheric ozone is considered in calculations of intensities of upward radiation emerging at the top of the atmosphere. (From supplemental tables to MSL Rep., 10.)

Our evaluation of limb darkening is obtained in the Africa case study and the results may, strictly speaking, be applied only to other situations where similar conditions in the atmosphere exist. However, the deviation between observed and theoretical values is probably much larger than a change in limb darkening caused by changes in the nature of the atmosphere. Therefore, if surface temperature is deduced from satellite measurements, the theoretical limb darkening will in all cases give too small corrections when measurements are made at zenith angles larger than 65 degrees. In our particular case, the temperatures measured above mountains in the Sahara Desert ranged from about 38 to 40 degrees Centigrade and the readings above the sand dunes usually indicate temperatures about five degrees lower.

Measurements were also carried out for channel 4, the broad channel covering the spectral region of 7 to 30 microns, and for channel 3, which measures reflected solar radiation and covers the spectral region between 0.25 and 6 microns. For these channels the degree of limb darkening was found to be smaller than that appearing in channel 2. On channel 4, however, it seems that a time lag effect exists due to the pen recorder, making

it is very difficult to interpret the measured values. Therefore small time lag effects in channels 2 and 3 probably occur, causing the limb darkening curve to fall off less steeply than expected if we judge from the curve's tendency at ζ ranging from 30 to 70 degrees. In this paper, work has been concentrated on finding the limb darkening in channel 2, but the more tentative results for channels 3 and 4 may have some other interest and are given in table II. Parentheses indicate where the influence of the time lag is serious.

TABLE II. Observed limb darkening. Channels III and IV TIROS III over Sahara.

ζ in deg.	\bar{W}/\bar{W}_0 CH. 3	\bar{W}/\bar{W}_0 CH. 4
50	.98	(1.03)
60	.94	(1.02)
70	.86	0.92
80	.70	0.71
90	.47	(0.95)

V. REMARKS

As pointed out earlier in this paper one is able by this method to observe not more than twice a particular spot on the earth during the satellite's flight. We are forced to combine readings from pairs of measurements of radiation which originates in widely separate areas, despite the fact that a difference in the composition of the atmosphere in horizontal planes will influence the measured values of limb darkening. In particular, water vapor in the atmosphere will be of great importance because the wings of the water vapor bands are within the spectral response of channel 2. The 9.6 micron ozone band will also influence the upward radiation. However, over the areas used in this case, mostly the desert regions of Africa, one can assume that a stratified ozone layer exists.

Very little information about the water vapor content was available for the areas where limb darkening measurements were made. From ground observations, within the area and without, combined with balloon

soundings on the periphery, we obtained some information about the distribution of the water vapor in the atmosphere. In fig. 8, we have given a schematic view of the conditions in the atmosphere along a center line within the area of the measurements.

Over the area where measurements were made at ζ equal to 90 degrees, the atmosphere seemed to be relatively dry at the surface with a water vapor layer aloft. Water vapor mass gives a high degree of limb darkening when it is aloft because it is a cold absorber and therefore, the limb darkening may not be much greater in the area of 70 and 60 degrees zenith angle, where the water vapor mass is larger, but at a lower level. On the whole, the conditions for measuring limb darkening seemed to be reasonably favorable. The limb darkening curve, as given, represents a mean range, valid for a tropical and humid atmosphere.

It is difficult to explain the large deviation from the theoretical values which is observed at zenith angles of above 75 degrees in channel 2. One can presume no clouds exist in this case, suggesting the possibility that dust particles may be causing this effect, which could be in accordance with channel 3 measurements of upward radiation-- a subject we shall deal with in another paper.

APPENDIX

RESOLUTION OF THE RADIOMETER

When a beam of light illuminates the satellite sensor area one gets a response, R . Such a response will depend on the intensity I of the light, the sensitivity of the sensor, and the size of the illuminated sensor area. We denote the sensitivity by S , and assume this to be a function of r only, the radial distance from the aperture axis on the sensor. We may write:

$$R_1 = \int_0^{2\pi} \int_0^{r_1} I S r d\phi dr,$$

where R is the instrumental response and ϕ is the azimuth angle in the sensor plane. The ratio

$$\frac{R_1}{R_0} = \frac{\int_0^{r_1} S r dr}{\int_0^{r_0} S r dr},$$

expresses relative or normalized power output of the radiometer, and is geometrically represented by contours on the sensor area. An area surrounded by a specific power contour and projected on the earth is called a scan spot. The size of the scan spot will determine the resolution power of the radiometer; it is important therefore, to know the sensor's power contours. As a consequence of eq. 1, the sensitivity S , has to be known if we want the values of R .

The satellite's radiometer has been calibrated by moving a traveling slit over the sensor. If the effective length of the slit is denoted by l , the instrumental response in this experiment is expressed by

$$R = \Delta x \int_0^l I S dl,$$

where Δx is the width of the traveling slit focussed on the sensor. We are interested in the relative change of S only, and the response in relative or normalized units is given by

$$R_{REL} = \frac{R}{R_{MAX}} = \frac{\int_0^l S dl}{\int_0^{l_{MAX}} S dl},$$

and the values of S are found by solving the integral equation:

$$C_A = \int_0^l S dl ;$$

this is done numerically by considering the finite equation,

$$C_A \approx \sum_i S_i \Delta l ,$$

where C_A is taken in arbitrary units from the observed curve in the calibration measurements.

Through these computations we found the values of the sensitivity, in percent, as a function of the instrument's aperture angle, which were used as weighting factor for the evaluation of a weighted mean value over a scan spot. (See Fujita 1963b).

REFERENCES

- Elsasser, Walter M., 1942: Heat transfer by infrared radiation in the atmosphere. Harvard Met. Studies, 6.
- Fujita, T., 1963a: A technique for precise analysis for satellite data; Volume I Photogrammetry. MSL Rep. 14.
- , 1963b: Outline of a theory and examples for precise analysis of satellite radiation data. Mesomet. Res. Paper 15, University of Chicago.
- , 1963c: A technique for precise analysis of satellite photographs. Mesomet. Res. Paper 17, University of Chicago.
- Hanel, R.A. and D.Q. Wark, 1961: Physical significance of the TIROS II radiation experiment. NASA technical note D-701.
- National Aeronautic and Space Administration, 1962: TIROS III radiation data user's manual. Goddard Space Flight Center, Greenbelt, Maryland.
- Wark, D.Q., G. Yamamoto and T. Lienesch, 1962: Infrared flux and surface temperature determinations from TIROS radiometer measurements. MSL Rep. 10.
- Wark, 1963: Personal Communication.

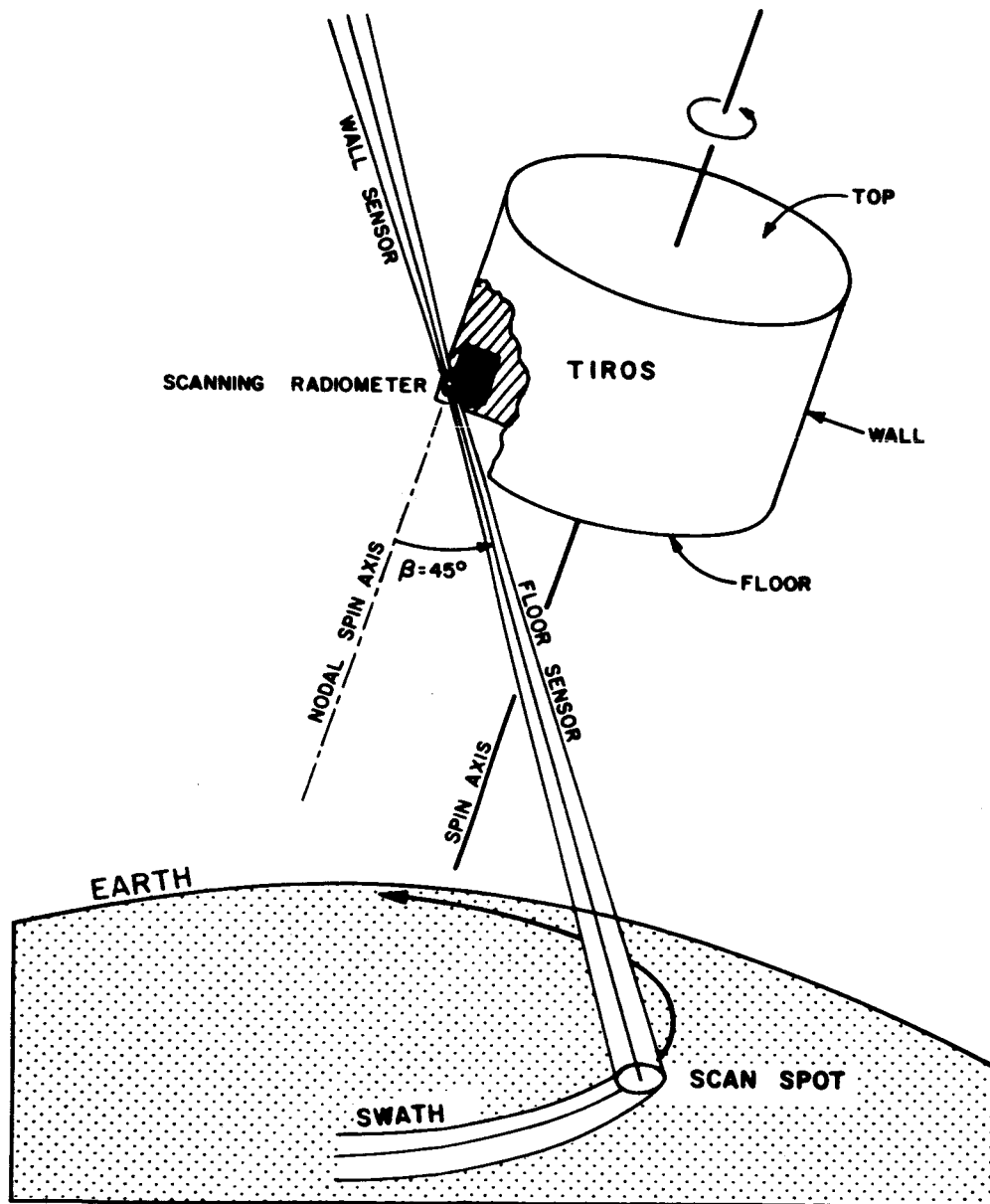


Fig. 1. Schematic view of TIROS III with its five-channel radiometer which scans the earth as it spins and progresses along its path. The radiometer beam has a 45 degree inclination to the spin axis which direction is fixed in space.

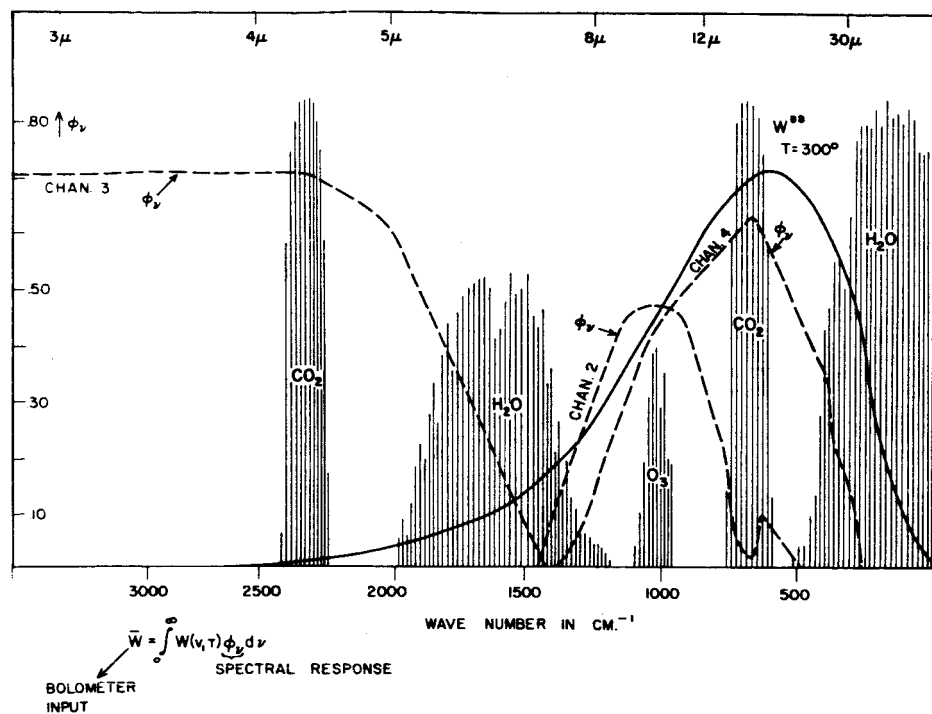


Fig. 2. Spectral response for the radiometer channels 2, 3, and 4, drawn on a diagram of principal absorption bands of the atmosphere in the infrared.

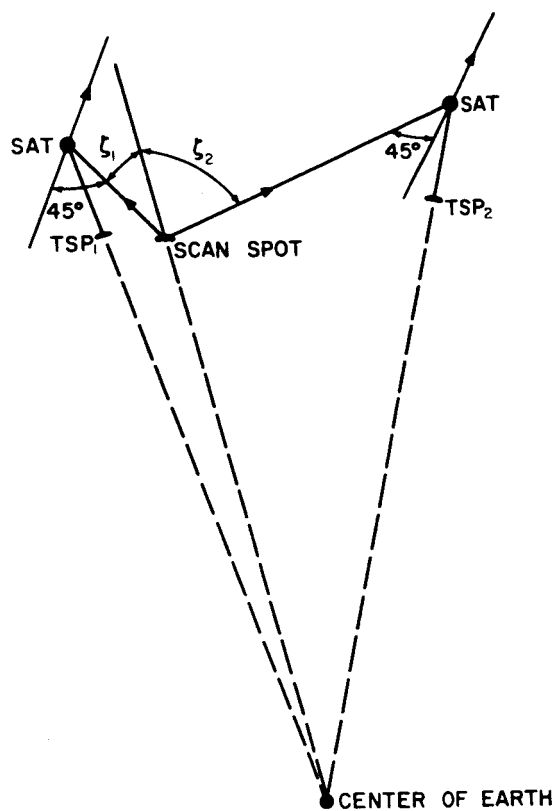


Fig. 3. Scan geometry of radiometer measurements one particular point on the earth is viewed by the satellite at two different zenith angles.

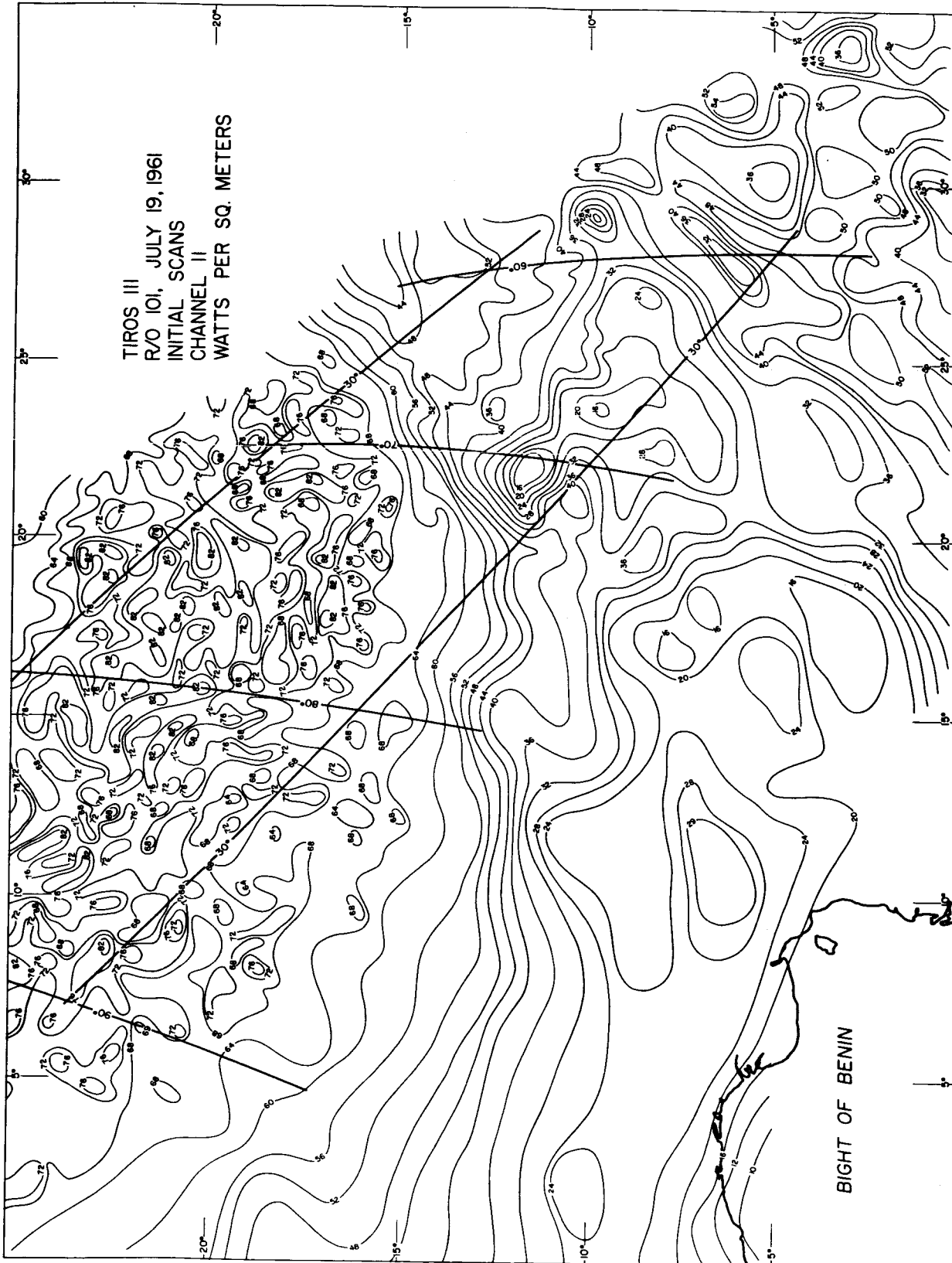


Fig. 4. Analysis of channel 2 (8 to 12 micron) radiation data from initial scans. The measurements made at small zenith angles.

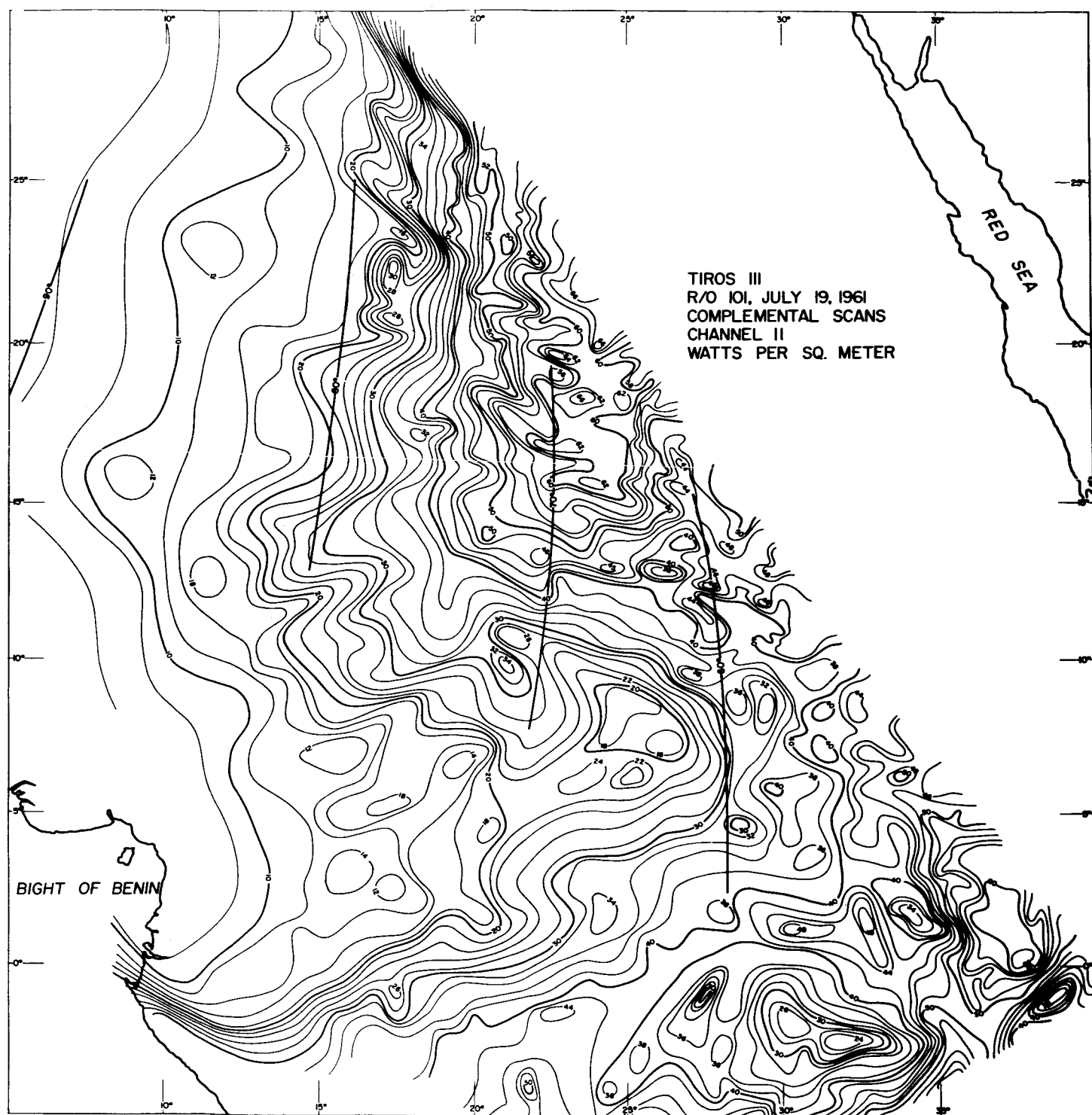


Fig. 5. Analysis of channel 2 (8 to 12 micron) radiation data from complemental scans. The measurements made at large zenith angles.

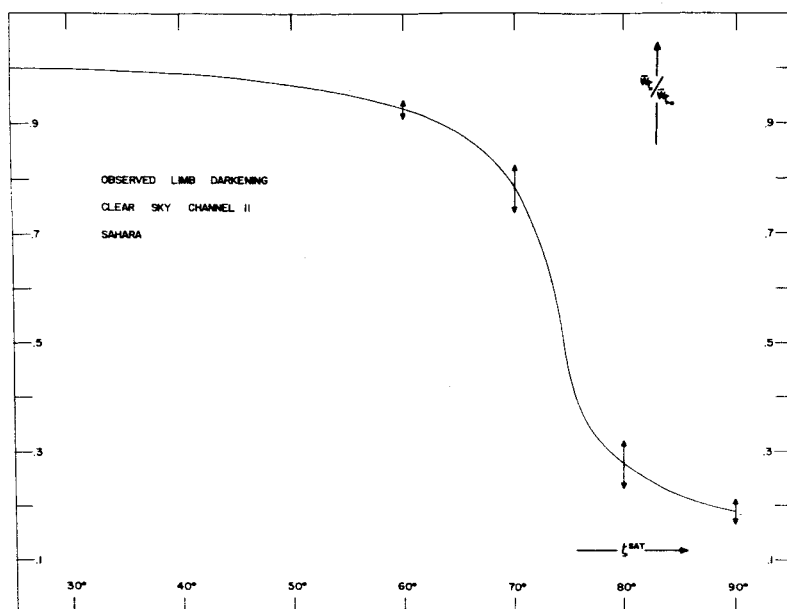


Fig. 6. Observed limb darkening, the measured ratio of the intensity of outgoing radiation at a zenith angle ξ to the intensity of outgoing radiation in the vertical, \bar{W}/\bar{W}_0 , as a function of ξ .

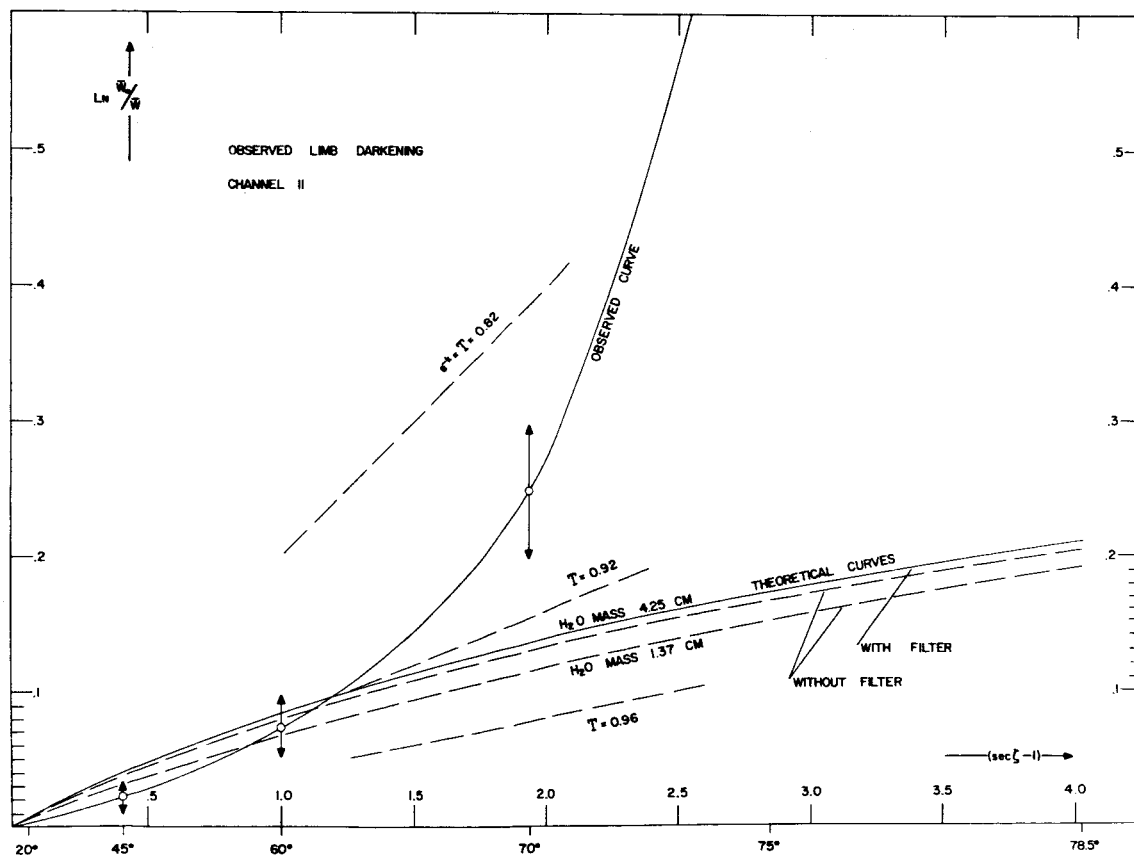


Fig. 7. The log intensity ratio $\log \bar{W}/\bar{W}_0$ plotted against (sec $\zeta - 1$) for measured and theoretical values of intensities of outgoing radiation.

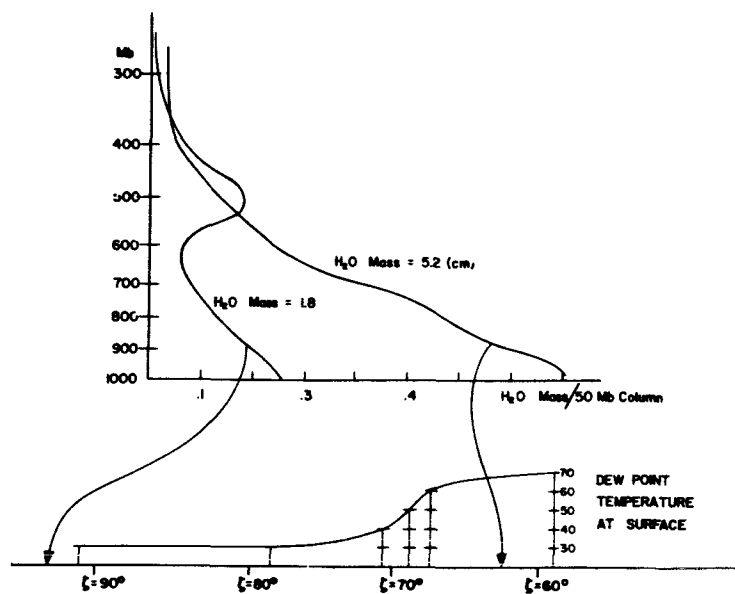


Fig. 8. Distribution of water vapor in the atmosphere in a cross section along the central area of observation. Dew point temperatures are given in degrees Fahrenheit.